Activation of the Crtc2/Creb1 transcriptional network in skeletal muscle enhances weight loss during intermittent fasting

Nelson E. Bruno[1]*, Jerome C. Nwachukwu[1], Sathish Srinivasan[1], Richard Hawkins, David Sturgill[3], Gordon L. Hager[3], Stephen Hurst[4], Shey-Shing Sheu[4], Michael D. Conkright[5], Kendall W. Nettles[1]*

[1]Department of Integrative Structural and Computational Biology, The Scripps Research Institute, 130 Scripps Way, Jupiter FL 33458, USA

[2]Department of Cancer Biology, The Scripps Research Institute, 130 Scripps Way, Jupiter FL 33458, USA

[3]Laboratory of Receptor Biology and Gene Expression, National Cancer Institute, NIH, Bethesda, MD 20892, USA

[4]Center for Translational Medicine, Department of Medicine, Thomas Jefferson University, Philadelphia, PA, 19107, USA.

[5]Department of Shared Services, The Scripps Research Institute, 130 Scripps Way, Jupiter FL 33458, USA

Correspondence: Nelson E Bruno, nbruno@scripps.edu; Kendall Nettles, knettles@scripps.edu

Conflict of interest statement: The authors declare no conflicts of interest.

Abstract

The Creb-Regulated Transcriptional Coactivator (Crtc) family of transcriptional coregulators drive Creb1-mediated transcription effects on metabolism in many tissues, but the in vivo effects of Crtc2/Creb1 transcription on skeletal muscle metabolism are not known. Skeletal muscle-specific overexpression of Crtc2 (Crtc 2 mice) induced greater mitochondrial activity, metabolic flux capacity for both carbohydrates and fats, improved glucose tolerance and insulin sensitivity, and increased oxidative capacity, supported by upregulation of key metabolic genes. Crtc2 overexpression led to greater weight loss during alternate day fasting (ADF), selective loss of fat rather than lean mass, supported by maintenance of higher energy expenditure during the fast. ADF downregulated most of the mitochondrial electron transport genes, and other regulators of mitochondrial function, that were substantially reversed by Crtc2-driven transcription. Glucocorticoids acted with AMPK to drive atrophy and mitophagy, which was reversed by Crtc2/Creb1 signaling. Crtc2/Creb1-mediated signaling coordinates metabolic adaptations in skeletal muscle that explain how Crtc2/Creb1 regulates metabolism and weight loss.

Key words: Crtc2; Creb1; skeletal muscle; intermittent fasting

37 **1. Introduction**

38 Long-term dieting is usually not effective in maintaining a lower body weight due to increased
39 hunger and a slower metabolic rate (1). In humans, loss of >10% of body weight also increases
40 metabolic efficiency, such that ~500 less calories per day are required to maintain the same
41 energy expenditure (2). Weight loss reduces the metabolic rate due to a number of changes
42 including increased circulating leptin and decreased thyroid hormone and sympathetic nervous
43 system (SNS) activity (2-4). People who maintain long-term weight loss almost invariably
44 exercise (5), and both preclinical and clinical data suggest that this is through raising metabolic
45 rate (6-8), decreased energy efficiency (9), and increased energy expenditure from the increased
46 physical activity (10).

47 Creb1-regulated transcription is stimulated by GPCRs, such as the β-adrenergic receptor
48 (βAR) during exercise (11-14), which activate adenylyl cyclases to convert ATP to the second
49 messenger cAMP, which in turn liberates the catalytic subunit of protein kinase A (PKA) (15).
50 Crtc1–3 family members are primary coactivators for Creb1 that are also highly conserved in the
51 cAMP transcriptional response. Crtc1–3 are rendered cytoplasmic and inactive by
52 phosphorylation (16). In contrast, they are fully activated through synergistic dephosphorylation
53 by phosphatases downstream of PKA and calcium flux in polarizable tissues including the
54 skeletal muscle (11), hippocampus (17), cortex (18), islet cells (16), and the renal proximal
55 tubule (19). In skeletal muscle, Crtc/Creb1 is activated by exercise downstream of the β-
56 adrenergic receptor and calcium flux (11), stimulating anabolic transcriptional programs (20),
57 including induction of PGC-1α (11, 21) and in vitro enhancement of oxidative capacity (21).
58 While Crtc/Creb1 coordinates metabolic transcriptional programs in other tissues such as
59 adipocytes, liver, and pancreas, its role in skeletal muscle metabolism has not been studied in

60 vivo.

61 To investigate the effects of Crtc2/Creb1 activation in adult skeletal muscle, we
62 generated doxycycline (dox)-inducible transgenic mice that show skeletal muscle-specific
63 overexpression of Crtc2 (FLAG-Crtc2 S171A/S275A/K628R mutant that prevents cytoplasmic
64 localization) under the control of a tetracycline response element (11). Induction of Crtc2
65 improved whole animal and skeletal muscle metabolism, enabling maintenance of higher energy
66 expenditure during fasting and improved weight loss.

67

68 **2. Materials and Methods**

69 **2.1 Statistical analyses**

70 Changes in body weight and body were analyzed with 2-way analysis of variance. For VO_2,
71 respiratory quotient, and ambulation data, the ad libitum and fasted periods were analyzed
72 separately with 2-way ANOVA, and the refeeding data analyzed with Student's T-test. For the
73 energy consumption data, the fasted and re-fed data were analyzed together with 2-way
74 ANOVA. Gene expression data were analyzed with 1-way ANOVA, with Dunnett's test for
75 multiple comparisons of each gene to its corresponding control. Glycemia and insulin changes
76 over time were analyzed with 2-way ANOVA, and the AUC assessed with Student's T-test. The
77 behavioral data for meal consumption were analyzed with Student's T-tests.

78

79 **2.2 Crtc2 transgenic mice and animal care**

80 All animal procedures were approved by the Scripps Research Institute ICACUC. TRE-Crtc2^{tm}
81 mice were generated by cloning FLAG-Crtc2 (S171A, S275A, K628R) into pTRE-Tight. Oocyte
82 injections were conducted into C57Bl6 at the University of Cincinnati. Double transgenic mice

83 (DTg) were generated by crossing C57BL/6-Tg(TRE-Crtc2tm)1Mdc/j mice with 1256[3Emut]
84 MCK-rtTA transgenic mice, which expresses the reverse tetracycline transactivator (rtTA)
85 regulated by the 1256[3Emut] MCK promoter specifically in skeletal muscle (Grill *et al*, 2003).
86 Wild type and TRE littermates were used as controls and treated with DOX in the same manner
87 as DTg mice. High fat diet (Research Diet D12450J) contained 60 kcal% fat and matched control
88 low fat diet (D12492) contained 10kCal% fat and 7% sucrose.
89

90 **2.3 Glucose and insulin tolerance tests**

91 Glucose tolerance testing was performed after an overnight fast. Blood glucose was quantified at
92 15, 30, 60, 90 and 120 min post-i.p. administration of 20% D-glucose (1 g/kg fasted body
93 weight) with an Accu-check glucose monitor as described (Heikkinen *et al*, 2007). Insulin
94 tolerance testing was performed on 6 hr-fasted mice injected i.p. with human insulin (1.5 U/kg
95 fasted body weight). Blood glucose levels were determined immediately before, and 15 and 30
96 min after, injection.
97

98 **2.4 In vivo electroporation**

99 Plasmid DNA (50 mg) was transfected into mouse tibialis anterior (TA) muscles by
100 electroporation as described previously (11). 1 hr before electroporation mice were anesthetized,
101 and a small incision was made through the skin covering the TA muscle and then injected with
102 30 Al of 0.5 U/Al hyaluronidase and then injected with plasmid DNA. *Crtc2* and *GFP*
103 expression plasmids were purified from DH5a *Escherichia coli* cultures using an EndoFree
104 plasmid kit (Qiagen, Valencia, CA, USA), and resuspended in 71 mM sterile PBS. After the
105 injections, electric pulses were administered by using non-invasive platinum-coated

106 tweezertrodes. Eight 100-ms square-wave electric pulses at a frequency of 1 Hz and at 200-ms
107 intervals were delivered with an ECM 830 electroporation unit (BTX-Harvard Apparatus,
108 Holliston, MA, USA) with a field strength of 40 V/cm. After the electroporation procedure, the
109 incision was closed with Vetbond surgical glue.
110

111 **2.5 Indirect calorimetry and energy expenditure**

112 Mice were individually housed in a sixteen chamber Oxymax comprehensive lab animal
113 monitoring system (CLAMS; Columbus Instruments, Columbus OH) at 26° C. Animals were
114 allowed to acclimate for 1 day followed by VO_2 and VCO_2 were measured at 13 min intervals
115 over a continuous duration of 60 hr. Energy expenditure (EE) was calculated using the Lusk
116 equation, kcal/h = (3.815 + 1.232 × RQ) × VO_2 in l/h, where RQ is the ratio of VCO_2 to VO_2.
117 Opto-Varimetrix-3 sensor system in the *x*-, *y*-, and *z*-axes of each chamber recorded sterotype,
118 ambulatory and *z*-axis activity. Consecutive adjacent infrared beam breaks in either the *x*- or *y*-
119 axes were scored as ambulatory activity.
120

121 **2.6 Body composition**

122 Body composition was determined using time domain nuclear magnetic resonance (TD-NMR) in
123 a Bruker minispec.
124

125 **2.7 Automated food intake monitoring**

126 Feeding behavior was assessed using a BioDAQ episodic Food Intake Monitor (BioDAQ,
127 Research Diets, Inc) as described (Stengel *et al*, 2010). Feeding parameters were calculated with
128 BioDAQ Monitoring Software 2.2.02. Feeding bouts were defined as a change in stable weight

129 of food. Meals consisted of two or more bouts within 5 s with a minimum meal amount of 0.02
130 g. Clusters of bouts occurring greater than 600 seconds apart were considered separate meals.
131 Water or water containing Dox was provided *ad libitum* from regular water bottles. Mice
132 habituated to the new environment within 1 day and showed normal food intake and regular
133 body weight gain.
134

135 **2.8 mRNA-seq and bioinformatics**

136 Total RNA was extracted from tissues using TRIzol™ reagent (Invitrogen), and cleaned up using
137 the RNeasy kit with on-column DNA digestion (QIAGEN). Three mRNA-seq libraries per
138 condition were prepared using the NEBNext Ultra II directional RNA library Prep kit for
139 Illumina (New England Biolabs), and read in paired-end 40-cycle sequencing runs on the
140 NextSeq 500 system (Illumina). Sequences were aligned to the Ensembl *Mus musculus*
141 GRCm38.83.chr.gtf genome (mm10) assembly using HISAT2 v2.0.5 (PMID: 25751142), sorted
142 and indexed using SAMtools v1.7 (22) and quantified for differential expression analysis using
143 Subread v1.6.1 featureCounts (23). Differential expression analysis was performed using
144 DESeq2 v1.18.1 (24, 25). Enriched canonical pathways were identified using the Ingenuity
145 pathways analysis software (QIAGEN). Gene Ontology (GO) analysis excluding inferred
146 electronic annotations, was performed using the Mouse Genome Informatics GO Browser and
147 GO Term Mapper (http://www.informatics.jax.org). Genes encoding mouse nuclear hormone
148 receptors were obtained from the Nuclear Receptor Signaling Atlas (NURSA) (26). Genes
149 encoding mitochondrial proteins were obtained from the mouse Mitocarta2.0 (27, 28). Genes
150 encoding transcriptional coregulators were obtained from the EpiFactors database (29).
151 Glucocorticoid-responsive genes were obtained by combining previously published datasets (30)

152 reanalyzed with GEO2R, with other dexamethasone-regulated genes that we identified in C2C12
153 myotubes, GEO accession no. GSE149453. Heatmaps were prepared using Pheatmap v1.0.8,
154 RColorBrewer v1.1–2, and other software packages available in R. Other data visualizations
155 were performed using GraphPad Prism7.
156

157 **2.9 Glucose uptake**

158 Insulin mediated 2-deoxy-D-[^{14}C] glucose uptake was determined by incubating primary
159 myotubes with PBS or PBS containing 100 nM insulin for 30 min followed by addition of 0.1
160 mM of cold 2-deoxy-D-glucose and 0.1μCi/well of 2-deoxy-[^{14}C] D-glucose for 5 min prior to
161 solubilization. Nonspecific deoxyglucose uptake was measured in the presence of 20 μM
162 cytochalasin B and subtracted from the total glucose uptake.
163

164 **2.10 Primary myoblast isolation and culture**

165 Primary myoblasts were isolated from P1 to P3 (1–3 day old) C57BL/6J pups as described
166 (Springer *et al*, 1997) and cultured on collagen coated plates in media consisting in 1:1 F-
167 10/DMEM supplemented with 20% FCS and 25 μg/ml bFGF. Subconfluent myoblasts were
168 differentiated into multinucleated myotubes using a 1:1 F-10/5 mM glucose DMEM
169 supplemented with 4% heat inactivated horse serum (Hyclone) for up to five days. For steroid-
170 free culture conditions, cells were grown in charcoal:dextran-stripped FBS (Gemini Bio-
171 products, cat no. 100-119).
172

173 **2.11 Adenoviruses**

174 Control GFP-expressing and Crtc2 expressing adenoviruses have been described (Koo *et al*,

175 2005; Wu *et al*, 2006). For all experiments myotubes were infected after 72 hr of differentiation
176 with 4×10^8 viral particles per ml per well for 24–48 hr.
177
178 **2.12 Immunoblotting analysis**
179 Immunoblot analysis was performed as described (Conkright *et al*, 2003a). Whole cell extracts
180 were prepared in HEPES whole cell lysis buffer (20 mM HEPES, pH 7.4, 1% TX-100,1x
181 phosphoSTOP complete inhibition cocktail tablets [Roche], and 1X Complete-EDTA Free
182 protease inhibitor cocktail [Roche]). Frozen muscle tissue was homogenized in lysis buffer T-
183 PER® Tissue Protein Extraction reagent (Thermo Scientific) by a polytron homogenizer and
184 sonication. The protein concentration was determined using the protein assay reagent (Bio-Rad).
185 60–80 μg of protein were separated by SDS-PAGE and transferred to nitrocellulose membranes
186 for immunoblotting. Nur77/Nr4a1 #2518 Rabbit polyclonal antibody was from Novus
187 Biological. CRTC2 #A300-638A Rabbit polyclonal antibody was from Bethyl Laboratories. Irs2
188 (L1326) #3089S Rabbit polyclonal antibody was Cell Signaling Technology, Inc. Tubulin
189 #T9026-.2ML Mouse Monoclonal antibody was from Sigma-Aldrich. pAKT(Thr308) (244f1)Rb
190 and pAKT(Ser473) (971s) were from Cell Signaling Technology. PGC1α ab54481 Rb was from
191 Abcam.
192
193 **2.13 Quantitative RT-PCR (qPCR)**
194 Total RNA from tissue or cells was harvested using Rneasy RNA Kit (Qiagen) and cDNA
195 prepared using Transcriptor High Fidelity cDNA Synthesis Kit (Roche). Relative abundance of
196 cDNAs was determined a Roche LightCycler 480, and the resulting data were normalized to *Rpl-*
197 *23* ribosomal RNA (IDT) as described (Conkright *et al*, 2003b). The primer pairs are as follows:

198 *Nr4a1* (5′-ttctgctcaggcctggtact′, 5′-gattctgcagctcttccacc-3′); *Nr4a3* (5′-tcagccttttggagctgtt′, 5′-
199 tgaagtcgatgcaggacaag-3′); *Irs2* (5′-acaacctatcgtggcacctc-3′, 5′-gacggtggtggtagaggaaa-3′); Idh3a
200 (5′-gtgacaagaggttttgctggt-3′, 5′-tgaaatttctgggccaattc-3′); *Cytc* (5′-gatgccaacaagaacaaaggt-3′, 5′-
201 tgggattttccaaatactccat-3′); *Glut4* (5′-tgtggctgtgccatcttg-3′, 5′-cagggccaatctcaaagaag-3′).
202

203 **2.14 Mitochondrial DNA (mt-DNA) analysis**

204 Total DNA was extracted using the GenElute™ mammalian genomic DNA miniprep kit (Sigma-
205 Aldrich). Triplicate real-time PCR reactions were performed using 50 ng of total DNA, *CoxI* (5′-
206 agcattcccacgaataaataaca-3′, 5′-agcattcccacgaataaataacat-3′) or *CoxII* (5′-tttcaacttggcttacaagacg-3′,
207 5′-tttcaacttggcttacaagacg-3′) mitochondrial DNA primers, and a control genomic DNA primer,
208 *Gapdh* (5’-gaaaaggagattgctacg-3’, 5’-gcaagaggctaggggc-3’).
209

210 **2.15 Histology**

211 Dissected muscle tissue was mounted in OCT medium (TissueTek) and froze in liquid N_2–
212 cooled isopentane. Tissue sections were stained for succinate dehydrogenase activity to
213 distinguish between oxidative and nonoxidative fibers using standard methods.
214

215 **2.16 Fatty acid metabolism**

216 Fatty acid oxidation was assayed by incubating (9,10(n)-^{3}H) palmitic acid (60 Ci/mmol) bound
217 to fatty-acid free albumin (final concentration:100 μM, palmitate:albumin 2:1) and 1 mM
218 carnitine with primary myocytes for 2 hr. Tritiated water released was collected and quantitated.
219

220 **2.17 High-content imaging and analysis**

221 Primary or C2C12 myotubes in black 96- or 384-well tissue culture plates with clear bases
222 (Greiner Bio-One, North America, Inc.) were stained for 15 min with 200 nM MitoTracker®
223 Orange CM-H_2TMRos dye (Invitrogen™ by ThermoFisher Scientific). The myotubes were
224 rinsed with steroid-free DMEM to remove un-incorporated dye, and then incubated in the
225 differentiation media for 45 min to reach peak fluorescence. Myotubes were fixed in 4%
226 formaldehyde for 20 min, stained with 300 nM DAPI for 5 min, permeabilized in PBS
227 containing 0.1% Triton X-100 for 20 min, blocked for 1 h with 1x TBS containing 0.1% Tween-
228 20 (TBS-T) and 2.5% normal goat serum, and incubated at 4°C overnight with an AlexaFluor®
229 488-conjugated anti-skeletal muscle myosin (F59) antibody (Santa Cruz Biotechnology, Inc. cat
230 no. sc-32732 AF488). The next day, the myotubes were washed 4 times with TBS-T to remove
231 unbound antibodies and rinsed twice with PBS. The stained myotubes were imaged at 10–20X
232 magnification on the IN Cell Analyzer 6000 platform (GE Healthcare). For each treatment
233 condition, a stack of 24–27 images containing an average of 50–100 myotubes per image were
234 analyzed using the IN Cell Developer Toolbox image analysis software, with a customized
235 segmentation protocol for myotubes. The average (mean) diameter and mitochondrial potential
236 (i.e. MitoTracker staining density x area) of myotubes in these images were then calculated.
237

238 **3. Results**

239 **3.1 Crtc2 stimulates mitochondrial activity and improves oxidative capacity**

240 After one week of dox treatment, Crtc2 mice showed increased mitochondrial succinate
241 dehydrogenase activity in the gastrocnemius muscle (**Figure 1A, Supplemental Fig. 1A–B**) while
242 myotubes overexpressing Crtc2 or Crtc3 oxidized more palmitate than control myotubes (**Figure**
243 **1B**), as previously reported (21). The Crtc2 mice displayed increased expression of *Cytochrome*

244 *C (Cycs)*, *Ppargc1a/*PGC-1α (as previously reported (11, 21), and *Nr4a3/*NOR-1 nuclear
245 receptor (**Figure 1C**) which induces mitochondrial biogenesis and increases oxidative capacity
246 (31, 32), and is induced by high intensity exercise (11). Crtc2 also upregulated the *Dgat1* gene
247 (**Figure 1C**), which is a direct Creb1 target gene (11), the product of which catalyzes a rate-
248 limiting step that increases IMTG stores. These mitochondria-related genes were also
249 upregulated in primary myotubes overexpressing Crtc2, indicating a skeletal muscle-intrinsic
250 effect of Crtc2 that mimics the effects of exercise (**Figure 1D**). We also observed a doubling of
251 mitochondrial DNA after in vivo electroporation of Crtc2 into skeletal muscle (**Figure 1E**).
252 These data support a model where exercise induced mitochondrial biogenesis uses Crtc2/PGC-
253 1α transcriptional control programs to upregulate mitochondrial biogenesis and oxidative
254 capacity.
255
256
257 **3.2 Crtc2 improves glucose tolerance and carbohydrate metabolism.**
258 To probe for Crtc2-dependent changes in carbohydrate metabolism, we performed glucose
259 tolerance tests comparing Crtc2 and WT mice. After one week of dox treatment, the Crtc2 mice
260 displayed significantly improved glucose disposal, including a dramatic improvement in their
261 ability to reduce glycemia (**Figure 2A, Supplemental Figure 2**), and required a lower insulin
262 excursion (**Figure 2B**). Crtc2 overexpression also improved insulin tolerance (**Figure 2C**). In
263 primary myotubes, expression of Crtc2 was sufficient to significantly increase the uptake of 2-
264 Deoxy-D-glucose (**Figure 2D**).
265 Crtc2 mice and Crtc2/3-overexpressing myotubes upregulated a number of carbohydrate
266 signaling genes in normal fed conditions at both the RNA and protein levels (**Figure 2E–H**),

267 including the glucose transporter, *Glut4*, whose insulin-dependent translocation to the membrane
268 drives glucose uptake into skeletal muscle, accounting for 80% of glucose disposal. The *Nr4a1*
269 gene encodes Nur77, a nuclear receptor family transcription factor that regulates transcriptional
270 programs for carbohydrate metabolism, lipolysis, and mitochondrial biogenesis (33), and is
271 upregulated by high intensity exercise or adrenergic signaling (11). *Irs2*, *Akt1*, and *Akt2* encode
272 core components of the insulin receptor signaling pathway that can coordinate anabolic signaling
273 and improve carbohydrate metabolism. We also identified a significant inhibition of myogenin
274 expression in the normal fed Crtc2 mice (**Figure 2E**), a primary driver of muscle atrophy during
275 fasting. To validate on target mechanism of action, we generated stable cell lines overexpressing
276 Crtc3, dominant negative A-Creb, or dominant negative Crtc2 expressing only the Creb binding
277 domain (16). These results demonstrate that A-Creb and dn-Crtc2 blocked basal expression of
278 PGC-1α, Irs2, and Akt2, and prevented phosphorylation of Akt1/2 at Thr308 (**Figure 2G–H**).
279 These experiments demonstrate that exercise coordinates beneficial metabolic responses that are
280 recapitulated by activation of skeletal muscle Crtc2/Creb1 transcriptional programs.
281

282 **3.3 Crtc2 overexpression in skeletal muscle facilitates weight loss**

283 We noticed during the GTTs that the Crtc2 mice tended to lose more weight after the overnight
284 fast, so we tested them in the context of a common dieting scheme of intermittent fasting. We
285 studied aged Crtc2 (rtTA/Crtc2^{tm}) or WT (rtTA/WT) mice, which in the C57BL/6 background
286 naturally gain fat mass as they age (18 weeks, 30–39 g, **Figure 3A**). During dox treatment, Crtc2
287 mice gained weight similarly to control WT mice (**Supplemental Fig. 3A**). When subject to
288 alternate day fasting (ADF), three separate cohorts of Crtc2 mice displayed significantly greater
289 and sustained weight loss than WT mice, with Crtc2 mice losing about twice as much weight in

290 each case, 9-14% of body weight (**Figure 3B, Supplemental Fig. 3B**).

291 After 3 weeks of ad libitum refeeding, the Crtc2 mice re-gained more weight to catch up
292 with the WT mice (**Figure 3C**), which may be due to the anabolic effects of higher insulin
293 sensitivity (**Figure 2**). We found that locomotion was similarly reduced in both groups during
294 the refeeding period (**Supplemental Fig. 3C**), the number of meals doubled in both groups,
295 while meal duration and number of bouts per meal declined similarly (**Figure 3D**). We observed
296 a reduction in kilocalories consumed in the Crtc2 relative to the WT group, which planned
297 comparisons demonstrated was significant only during the second ADF cycle, when the WT
298 mice increased consumption at a faster rate than the Crtc2 mice (**Figure 3D**). Increases in skeletal
299 muscle storage of glycogen and triglycerides associated with the anabolic phenotype of
300 Crtc2/Creb1 activation (11) likely contributed to the early response to fasting, perhaps explaining
301 the initially slower rate of increased food consumption in the Crtc2 mice. These differences in
302 caloric consumption are consistent with the differences in body weight between cohorts and
303 disappear after normalization for body weight. However, control mice lost more lean mass, while
304 Crtc2 mice conserved lean mass and burned the excess fat accumulated during aging (**Figure**
305 **3E**), similar to the effects of exercise (34). To verify that Crtc2 helps maintain lower body
306 weight in a different model, we placed mice on a high fat diet, and found that Crtc2 mice also
307 maintained lower body weight than WT mice in this context (**Figure 3F**). To test for pre-fasting
308 changes in the central control of feeding and energy expenditure, we completed a leptin infusion
309 study, as leptin secretion from adipocytes both suppresses hunger and stimulates the SNS. The WT
310 and Crtc2 mice displayed identical patterns of weight loss following leptin infusion
311 (**Supplemental Figure 4D**), and there were also no differences in plasma levels of feeding
312 hormones, cholesterol, or triglycerides (**Supplemental Fig. 4E–F**). Thus, the activation of

313 Crtc2/Creb1 signaling in skeletal muscle significantly modulated body composition and weight
314 loss, mimicking the effects of exercise training including preferential loss of fat mass.
315
316 **3.4 Crtc2 maintains energy expenditure during fasting**
317 Lowered metabolic rate is one of the major defenses against fasting-induced weight loss. As
318 expected, ad libitum oxygen consumption cycled with activity in the mice, which increased at
319 night and decreased during the day (**Figure 4A, Supplemental Fig. 4A**). Fasting reduced oxygen
320 consumption at every cycle, and this effect was more pronounced during the day as the fast was
321 extended (**Figure 4A**). However, Crtc2 mice consistently showed higher oxygen consumption,
322 independent of fasting (**Figure 4A**).
323 When fed ad libitum, Crtc2 and control mice display similar rates of energy expenditure
324 (EE) (**Figure 4B**). We calculated EE from indirect calorimetry measurements of VO_2 and VCO_2
325 and performed ANCOVA analysis using body weight and NMR data as covariates to adjust the
326 EE to total body weight and body composition (**Supplemental Fig. 4B**). While fasting, the EE of
327 WT mice dropped significantly. In contrast, during fasting EE in Crtc2 mice did not drop below
328 the ad libitum levels (**Figure 4B**). Respiratory quotient was also reduced during fasting,
329 indicating greater utilization of fat for fuel, but the differences between WT and Crtc2 mice were
330 not significant (**Figure 4C, Supplemental Fig. 4C**). Maintenance of a higher energy expenditure
331 during fasting thus links Crtc2 activity to increased weight loss during fasting.
332
333 **3.5 The transcriptional response to fasting and weight loss and its regulation by Crtc2**
334 To understand the skeletal muscle intrinsic effects of Crtc2 on dieting and weight loss, we
335 performed transcriptional profiling of mice tibialis anterior (TA) muscles electroporated with

336 control and Crtc2 expression plasmids in contralateral legs. One cohort of electroporated mice was
337 subject to 3 cycles of ADF, while the other cohort was fed ad libitum. TA muscle tissues were
338 collected from both cohorts at the end of the third 24-hr fast. The transduction increased *Crtc2*
339 mRNA levels by ~2.5-fold across groups (**Figure 5A**). In response to ADF, we identified 1,880
340 differentially expressed genes (DEGs) in the control-transduced muscle and 3,197 DEGs in Crtc2-
341 transduced muscle, with 1,380 genes in common between the two groups (**Figure 5B**). Analysis of
342 canonical signaling pathways and gene ontology (GO) annotations revealed that ADF modulated
343 the transcriptional programs for lipid and carbohydrate metabolism, fatty acid beta-oxidation, and
344 insulin signaling (**Figure 5C–F,** annotated gene lists are in **Supplemental Dataset1**). ADF also
345 regulated transcriptional programs that control protein balance, including autophagy and ubiquitin-
346 dependent proteasomal degradation, RNA splicing, and transcription (**Figure 5C-D**). There were
347 also over 200 DEGs regulated by ADF that were annotated as transcription factors and
348 transcriptional coregulators along with > 50 transcription factor and coregulators altered by Crtc2
349 over-expression (**Figure 3G–I**), demonstrating the complexity of the transcriptional response to
350 intermittent fasting in skeletal muscle.

351 We considered that Crtc2 might be regulating secreted proteins that modulate the response to
352 dieting, using the Metazoan Secretome Knowledgebase (35). Among 2,500 genes encoding likely
353 secreted proteins, 171 DEGs were regulated by Crtc2 during ADF **(**Secretome, **Supplemental**
354 **Dataset1)**. Using the Reactome.org peer-reviewed pathway database, we detected significant
355 enrichment of pathways regulating extracellular matrix, inter-cell signaling, and immune function,
356 among others (**Supplemental Table 1**), but no changes in myokines that would drive weight loss.
357 However, Crtc2 signaling in skeletal muscle would be expected to have effects on other tissues just
358 from changes in skeletal muscle metabolic flux capacity (**Figures 1-2**).

359

360 **3.6 Crtc2 reverses fasting-induced effects on mitochondria**

361 In addition to lower metabolic rate, fasting and weight loss render humans and other mammals
362 more energetically efficient, such that the same amount of work is performed with less ATP
363 production, suggesting a remodeling of glycolytic or oxidative capacity (2, 36). ADF modulated
364 the expression of >200 genes whose proteins localize in mitochondria according to MitoCarta (27)
365 (**Figure 6A**). ADF downregulated most of the genes that encode the electron transport chain
366 (complexes I–IV), the ATP synthase (complex V), the mitoribosome, and the cytosolic ribosome
367 (**Figure 6A-C**, **Supplemental Fig. 5**), but significantly upregulated genes such as *Sdha*, *Uqcrc1*,
368 and *Atp5a1* (**Figure 6B**, **Supplemental Fig. 5**).

369 We observed a significant ADF-induced expression of genes encoding ROS scavenger
370 proteins such as thioredoxin (*Txnrd1*) and catalase (*Cat*), and genes regulating mitochondrial
371 stability*, Tomm7, Timm9,* and the AAA protease *Spg,7* known to be active during the removal of
372 damaged mitochondrial proteins (**Figure 6D**). Among the ATP synthase genes, there was a more
373 pronounced loss of gene expression in the lateral stalk genes (**Figure 6B**), which may decrease the
374 conductance of mitochondrial permeability transition pore (mPTP) and thus protect mitochondria
375 from detrimental swelling and oxidative injury (37). ADF also induced increases in mitochondrial
376 fusion (*Mfn2* and *Opa1)*, and decreased fission (*Fis)* gene expression, consistent with the
377 protective effects of fusion during nutrient deprivation (38). These adaptations could be
378 advantageous for weight loss as they prepare the mitochondria for the reduced metabolic rate and
379 increased reliance on lipid metabolism during fasting, without causing permanent damage to the
380 mitochondrial pool within the cell.

381 In mice subjected to ADF, Crtc2 transduction altered expression of 80 genes whose

382 proteins localize in the mitochondria. Crtc2 expression strongly attenuated the ADF-dependent
383 repression of electron transport chain genes and the mitoribosome (**Figure 6A–C**, **Supplemental**
384 **Fig. 5**), and generally upregulated the other genes encoding proteins that localize to mitochondria.
385 In addition, Crtc2 enhanced expression of ribosomal genes that facilitate mitoribosome assembly,
386 and genes such as *Spg7, Pink1, RhoT2*, and *Chchd3* that control the quality of mitochondrial
387 proteins, but blocked ADF-dependent downregulation of *Minos1*, a central component of the
388 mitochondrial inner membrane organizing system (**Figure 6D**). Crtc2 also upregulated expression
389 of *Tefm*, the mitochondrial transcriptional elongation factor, and *Bola3*, which participates in
390 electron transport chain assembly (39). These data suggest potential mechanisms to explain how
391 physical activity—through Crtc2/Creb1-regulated transcriptional programs—can help maintain a
392 higher metabolic rate and a lower body weight by upregulating expression of mitochondrial
393 respiratory chain subunits and modulating expression of other mitochondria-localized gene
394 products, consistent with the well-known beneficial effects of exercise on mitochondrial biogenesis
395 and energy expenditure.
396

397 **3.7 Crtc2 reverses catabolic effects of glucocorticoids on skeletal muscle**

398 To further understand the signaling pathways that are regulated by fasting and Crtc2, we noted
399 that glucocorticoids (GCs) are one of the primary drivers of systemic catabolism during fasting.
400 In response to ADF and Crtc2 overexpression, we observed over a thousand DEGs that were
401 annotated as "glucocorticoid response" genes (**Figure 5C**). In the context of an overnight fast,
402 treatment with dexamethasone (Dex) more than doubled loss of lean mass (**Figure 7A**). Using
403 high-content imaging, we observed that Dex reduced the diameter and mitochondrial potential of
404 nutrient-deprived primary mouse skeletal myotubes (**Figure 7B**). GCs can also activate the

405 master energy sensor, AMP-activated protein kinase (AMPK) (40), which can act as a
406 glucocorticoid receptor (GR) coactivator (41). AMPK is activated by a lower ATP/ADP ratio
407 during fasting to inhibit anabolism and stimulate catabolic processes such as autophagy and
408 mitophagy. In primary myotubes, we observed a Dex-dependent activating phosphorylation of
409 AMPK that increased over time, consistent with an underlying transcriptional mechanism
410 (**Figure 7C**). Activation of AMPK with both Dex and the AMP analog, AICAR, had an additive
411 detrimental effect on myotube diameter (**Figure 7D**), demonstrating that GR collaborates with
412 AMPK to drive skeletal muscle atrophy. To show that glucocorticoids and Crtc2 are directly
413 opposing each other in skeletal muscle, we transduced myotubes with Crtc2 expressing
414 adenovirus, which increased tube diameter, effects that were reversed by treatment of the cells
415 with Dex (**Figure 7E**). Importantly, the dominant negative A-Creb significantly reduced tube
416 diameter, demonstrating that Crtc2 is acting through Creb1 to regulated anabolic effects.
417
418
419 **Discussion**
420 This work reveals mechanisms through which Crtc2-induced transcriptional programs dramatically
421 rewire metabolism to regulate energy expenditure and the response to dieting. Crtc2 stimulated
422 mitochondrial biogenesis and activity, upregulated β-oxidation genes, increased lipid flux capacity,
423 improved insulin sensitivity and glucose disposal, and maintained higher energy expenditure during
424 fasting, phenocopying metabolic effects of exercise. Overexpression of PGC-1α increases
425 mitochondrial density and exercise performance, but without the increase in metabolic rate that can
426 occur from exercise training (42-45), highlighting the requirement for additional exercised-induced
427 signals. Transcriptional profiling revealed a profound effect of Crtc2 that prevented the ADF-

428 dependent loss of mitochondrial electron transport chain gene expression and opposed catabolic
429 effects of glucocorticoids that are induced by fasting. Crtc2/Creb1 metabolic rewiring enabled
430 greater weight loss during dieting, providing a mechanism for how exercise facilitates weight loss.

431 This work adds to a body of evidence on Crtc2 and Creb1 as global regulators of
432 metabolism in liver, pancreas, adipose tissue, and other endocrine tissues by coordinating with
433 other tissue- and stressor-specific transcriptional signaling programs. We previously demonstrated
434 that Creb1 and GR *work together* to coordinate gluconeogenesis transcriptional programs in the
435 liver, where GR doubles the number of Creb1 binding sites and increases binding of Creb1 (46).
436 We recently found that effects of GR ligands in skeletal muscle coordinately regulate inhibition of
437 AKT and new protein synthesis, while stimulating mitophagy and protein degradation, but used
438 different transcriptional pathways to inhibit insulin-mediated glucose uptake (accepted at *Nat*
439 *Chem Biol,* posted on bioRxiv https://doi.org/10.1101/2020.06.15.153270). This work suggests
440 that the effects of exercise on fasting may also involve a coordination of Creb1 and GR signaling
441 as master transcriptional regulators of metabolism, in conjunction with other stress-response
442 signals.

443 Reduced energy expenditure and increased hunger during fasting are partly mediated by a
444 lowering of the satiety hormone leptin (2-4). Leptin is also secreted basally from adipose tissue in
445 proportion to fat mass, so it is chronically lower during fasting, which lowers sympathetic tone and
446 energy expenditure, thyroid hormone levels, and stimulating the HPA axis (47)(**Figure 8A**).
447 Within skeletal muscle, increased glucocorticoids and AMPK activity are sufficient to reduce
448 mitochondrial potential (**Figure 7)**, which along with likely contributions from fasting-induced
449 lowering of thyroid hormone, bAR, and insulin receptor activity, induce mitochondrial dynamics
450 and mitophagy (**Figure 8A**).

451 These energetic effects of fasting are reversed by exercise (**Figure 8B**), which we now show
452 can be recapitulated by enforced expression of Crtc2/Creb1 and associated upregulation of
453 mitochondrial biogenesis master regulatory genes, *Nr4a1*, *Nr4a3*, *Essrra/*ERRα, and
454 *Ppargc1a/*PGC-1α (**Figure 1**). The combination of bAR and Ca^{2+} signaling are required to
455 maximally stimulate nuclear translocation of Crtc2 in skeletal muscle (11). In this model, increased
456 GC and AMPK activity during exercise promotes mitochondrial dynamics, which is then coupled
457 with mitochondrial biogenesis to increase mitochondrial potential and mass, in coordination with
458 other metabolic changes (**Figures 4–5**). Overexpression of Crtc2 circumvented the neuronal
459 activation of Creb1, as Crtc2 mice had most of the hallmarks of exercise adaptations before fasting
460 and weight loss (**Figures 4–5,** SI Appendix, **Figure S5B–C**), including increased exercise
461 performance, myotube diameter, and storage of IMTG and glycogen (11). As the SNS is activated
462 logarithmically in response to exercise intensity, Crtc2/Creb1 are likely driving responses to
463 novel exercise, leading to both anabolic and metabolic reprogramming.
464
465
466 **Data Availability**
467 The raw and processed RNA-seq dataset available at the National Center for Biotechnology
468 Information (NCBI) Gene Expression Omnibus (GEO) https://www.ncbi.nlm.nih.gov/geo/ and
469 can be retrieved with the accession number GSE149150, which will be released upon publication
470 of this manuscript. The processed RNA-seq dataset is also provided in SI Appendix, **Dataset S1**.
471 Relevant protocols and raw data not detailed in the Methods or Supplementary Information are
472 available upon request.
473
474 **Acknowledgements**. N.E.B. was supported by the BallenIsles Men's Golf Association. J.C.N. was

475 supported by the Frenchman's Creek Women for Cancer Research.

476

477 **Author contributions** Conceptualization, N.E.B., M.D.C., K.W.N.; Methodology, N.E.B.,

478 M.D.C.; Investigation, N.E.B., J.C.N., S.S., R.H., D.S.; Writing – Original Draft, K.W.N., N.E.B.,

479 M.D.C., S.H., S.S.S.; Writing – Revision, K.W.N, J.C.N., N.E.B.; Supervision, M.D.C, G.L.H.,

480 K.W.N., S.S.S., N.E.B.

481

482 **References**

483 1. C. L. Melby, H. L. Paris, R. M. Foright, J. Peth, Attenuating the Biologic Drive for Weight
484 Regain Following Weight Loss: Must What Goes Down Always Go Back Up? *Nutrients* **9**
485 (2017).
486 2. M. Rosenbaum *et al.*, Effects of experimental weight perturbation on skeletal muscle work
487 efficiency in human subjects. *Am J Physiol Regul Integr Comp Physiol* **285**, R183-192
488 (2003).
489 3. L. J. Arone, R. Mackintosh, M. Rosenbaum, R. L. Leibel, J. Hirsch, Autonomic nervous
490 system activity in weight gain and weight loss. *Am J Physiol* **269**, R222-225 (1995).
491 4. M. Rosenbaum *et al.*, Low-dose leptin reverses skeletal muscle, autonomic, and
492 neuroendocrine adaptations to maintenance of reduced weight. *J Clin Invest* **115**, 3579-
493 3586 (2005).
494 5. R. M. Foright *et al.*, Is regular exercise an effective strategy for weight loss maintenance?
495 *Physiol Behav* **188**, 86-93 (2018).
496 6. P. S. MacLean *et al.*, Regular exercise attenuates the metabolic drive to regain weight after
497 long-term weight loss. *Am J Physiol Regul Integr Comp Physiol* **297**, R793-802 (2009).
498 7. Y. Turk *et al.*, High intensity training in obesity: a Meta-analysis. *Obesity science &*
499 *practice* **3**, 258-271 (2017).
500 8. A. Mourier *et al.*, Mobilization of visceral adipose tissue related to the improvement in
501 insulin sensitivity in response to physical training in NIDDM. Effects of branched-chain
502 amino acid supplements. *Diabetes care* **20**, 385-391 (1997).
503 9. M. Rosenbaum *et al.*, Resistance Training Reduces Skeletal Muscle Work Efficiency in
504 Weight-Reduced and Non-Weight-Reduced Subjects. *Obesity (Silver Spring)* **26**, 1576-
505 1583 (2018).
506 10. D. M. Ostendorf *et al.*, Physical Activity Energy Expenditure and Total Daily Energy
507 Expenditure in Successful Weight Loss Maintainers. *Obesity (Silver Spring)* **27**, 496-504
508 (2019).
509 11. N. E. Bruno *et al.*, Creb coactivators direct anabolic responses and enhance performance
510 of skeletal muscle. *The EMBO journal* **33**, 1027-1043 (2014).
511 12. D. V. Popov *et al.*, Contractile activity-specific transcriptome response to acute endurance
512 exercise and training in human skeletal muscle. *Am J Physiol Endocrinol Metab* **316**, E605-
513 E614 (2019).
514 13. B. Egan *et al.*, Exercise intensity-dependent regulation of peroxisome proliferator-
515 activated receptor coactivator-1 mRNA abundance is associated with differential activation
516 of upstream signalling kinases in human skeletal muscle. *J Physiol* **588**, 1779-1790 (2010).
517 14. D. V. Popov *et al.*, Effect of aerobic training on baseline expression of signaling and
518 respiratory proteins in human skeletal muscle. *Physiological reports* **6**, e13868 (2018).
519 15. D. A. Walsh, J. P. Perkins, E. G. Krebs, An adenosine 3',5'-monophosphate-dependant
520 protein kinase from rabbit skeletal muscle. *The Journal of biological chemistry* **243**, 3763-
521 3765 (1968).
522 16. R. A. Screaton *et al.*, The CREB coactivator TORC2 functions as a calcium- and cAMP-
523 sensitive coincidence detector. *Cell* **119**, 61-74 (2004).
524 17. T. H. Ch'ng *et al.*, Activity-dependent transport of the transcriptional coactivator CRTC1
525 from synapse to nucleus. *Cell* **150**, 207-221 (2012).

18. P. S. Baxter, M. A. Martel, A. McMahon, P. C. Kind, G. E. Hardingham, Pituitary adenylate cyclase-activating peptide induces long-lasting neuroprotection through the induction of activity-dependent signaling via the cyclic AMP response element-binding protein-regulated transcription co-activator 1. *J Neurochem* **118**, 365-378 (2011).
19. M. Taub, S. Garimella, D. Kim, T. Rajkhowa, F. Cutuli, Renal proximal tubule Na,K-ATPase is controlled by CREB-regulated transcriptional coactivators as well as salt-inducible kinase 1. *Cell Signal* **27**, 2568-2578 (2015).
20. R. Berdeaux, C. Hutchins, Anabolic and Pro-metabolic Functions of CREB-CRTC in Skeletal Muscle: Advantages and Obstacles for Type 2 Diabetes and Cancer Cachexia. *Front Endocrinol (Lausanne)* **10**, 535 (2019).
21. Z. Wu *et al.*, Transducer of regulated CREB-binding proteins (TORCs) induce PGC-1alpha transcription and mitochondrial biogenesis in muscle cells. *Proc Natl Acad Sci U S A* **103**, 14379-14384 (2006).
22. H. Li *et al.*, The Sequence Alignment/Map format and SAMtools. *Bioinformatics* **25**, 2078-2079 (2009).
23. Y. Liao, G. K. Smyth, W. Shi, featureCounts: an efficient general purpose program for assigning sequence reads to genomic features. *Bioinformatics* **30**, 923-930 (2014).
24. M. I. Love, W. Huber, S. Anders, Moderated estimation of fold change and dispersion for RNA-seq data with DESeq2. *Genome Biol* **15**, 550 (2014).
25. S. Anders, W. Huber, Differential expression analysis for sequence count data. *Genome Biol* **11**, R106 (2010).
26. R. N. Margolis, R. M. Evans, B. W. O'Malley, N. A. Consortium, The Nuclear Receptor Signaling Atlas: development of a functional atlas of nuclear receptors. *Mol Endocrinol* **19**, 2433-2436 (2005).
27. S. E. Calvo, K. R. Clauser, V. K. Mootha, MitoCarta2.0: an updated inventory of mammalian mitochondrial proteins. *Nucleic Acids Res* **44**, D1251-1257 (2016).
28. D. J. Pagliarini *et al.*, A mitochondrial protein compendium elucidates complex I disease biology. *Cell* **134**, 112-123 (2008).
29. Y. A. Medvedeva *et al.*, EpiFactors: a comprehensive database of human epigenetic factors and complexes. *Database (Oxford)* **2015**, bav067 (2015).
30. T. Kuo *et al.*, Genome-wide analysis of glucocorticoid receptor-binding sites in myotubes identifies gene networks modulating insulin signaling. *Proc Natl Acad Sci U S A* **109**, 11160-11165 (2012).
31. J. C. Drake, R. J. Wilson, Z. Yan, Molecular mechanisms for mitochondrial adaptation to exercise training in skeletal muscle. *FASEB J* **30**, 13-22 (2016).
32. M. A. Pearen, G. E. Muscat, Minireview: Nuclear hormone receptor 4A signaling: implications for metabolic disease. *Mol Endocrinol* **24**, 1891-1903 (2010).
33. M. A. Maxwell *et al.*, Nur77 regulates lipolysis in skeletal muscle cells. Evidence for cross-talk between the beta-adrenergic and an orphan nuclear hormone receptor pathway. *The Journal of biological chemistry* **280**, 12573-12584 (2005).
34. R. J. Verheggen *et al.*, A systematic review and meta-analysis on the effects of exercise training versus hypocaloric diet: distinct effects on body weight and visceral adipose tissue. *Obes Rev* **17**, 664-690 (2016).
35. J. Meinken, G. Walker, C. R. Cooper, X. J. Min, MetazSecKB: the human and animal secretome and subcellular proteome knowledgebase. *Database (Oxford)* **2015** (2015).

571 36. R. Goldsmith *et al.*, Effects of experimental weight perturbation on skeletal muscle work
572 efficiency, fuel utilization, and biochemistry in human subjects. *Am J Physiol Regul Integr*
573 *Comp Physiol* **298**, R79-88 (2010).
574 37. V. Giorgio *et al.*, Dimers of mitochondrial ATP synthase form the permeability transition
575 pore. *Proc Natl Acad Sci U S A* **110**, 5887-5892 (2013).
576 38. A. S. Rambold, B. Kostelecky, N. Elia, J. Lippincott-Schwartz, Tubular network formation
577 protects mitochondria from autophagosomal degradation during nutrient starvation. *Proc*
578 *Natl Acad Sci U S A* **108**, 10190-10195 (2011).
579 39. V. Nasta, D. Suraci, S. Gourdoupis, S. Ciofi-Baffoni, L. Banci, A pathway for assembling
580 [4Fe-4S](2+) clusters in mitochondrial iron-sulfur protein biogenesis. *FEBS J*
581 10.1111/febs.15140 (2019).
582 40. J. Liu *et al.*, Mitochondrial Dysfunction Launches Dexamethasone-Induced Skeletal
583 Muscle Atrophy via AMPK/FOXO3 Signaling. *Mol Pharm* **13**, 73-84 (2016).
584 41. D. Ratman *et al.*, Chromatin recruitment of activated AMPK drives fasting response genes
585 co-controlled by GR and PPARalpha. *Nucleic Acids Res* **44**, 10539-10553 (2016).
586 42. C. S. Choi *et al.*, Paradoxical effects of increased expression of PGC-1alpha on muscle
587 mitochondrial function and insulin-stimulated muscle glucose metabolism. *Proc Natl Acad*
588 *Sci U S A* **105**, 19926-19931 (2008).
589 43. M. Tadaishi *et al.*, Skeletal muscle-specific expression of PGC-1alpha-b, an exercise-
590 responsive isoform, increases exercise capacity and peak oxygen uptake. *PLoS One* **6**,
591 e28290 (2011).
592 44. R. P. Shook *et al.*, Moderate cardiorespiratory fitness is positively associated with resting
593 metabolic rate in young adults. *Mayo Clin Proc* **89**, 763-771 (2014).
594 45. M. Gilliat-Wimberly, M. M. Manore, K. Woolf, P. D. Swan, S. S. Carroll, Effects of
595 habitual physical activity on the resting metabolic rates and body compositions of women
596 aged 35 to 50 years. *J Am Diet Assoc* **101**, 1181-1188 (2001).
597 46. I. Goldstein *et al.*, Transcription factor assisted loading and enhancer dynamics dictate the
598 hepatic fasting response. *Genome Res* **27**, 427-439 (2017).
599 47. R. J. Perry *et al.*, Leptin's hunger-suppressing effects are mediated by the hypothalamic-
600 pituitary-adrenocortical axis in rodents. *Proc Natl Acad Sci U S A* **116**, 13670-13679
601 (2019).
602

603

604 **FIGURES**

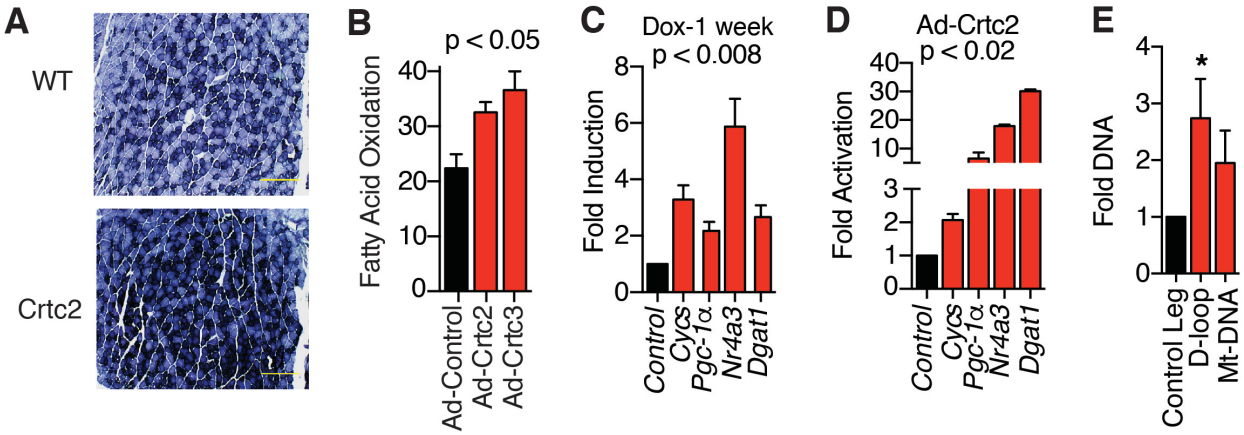

605

606 **Figure 1. Crtc2 expression in skeletal muscle enhances mitochondrial biogenesis.**

607 (**A**) Histological analysis of succinate dehydrogenase in myofibers from gastrocnemius muscle
608 sections after dox treatment. Scale bar = 500 μm.

609 (**B**) Oxidation of ^{3}H-Palmitic acid in the supernatant of primary myocytes transduced with
610 control, Crtc2, or Crtc3-expressing adenovirus.

611 (**C**) Gene induction calculated relative to WT mice. *N* = 8 mice per group.

612 (**D**) Gene expression in primary myocytes transduced with adenovirus expressing Crtc2 or GFP
613 control 72 hr post-transduction.

614 (**E**) Crtc2 expression plasmid was electroporated into the tibialis anterior muscle and GFP
615 plasmid in the contralateral leg. After 7 days, DNA was extracted for assessment of
616 mitochondrial DNA (mt-DNA) for Crtc2/GFP control. *N* = 5 mice per group.

617 * $p < 0.05$. Data are shown as mean + SEM.

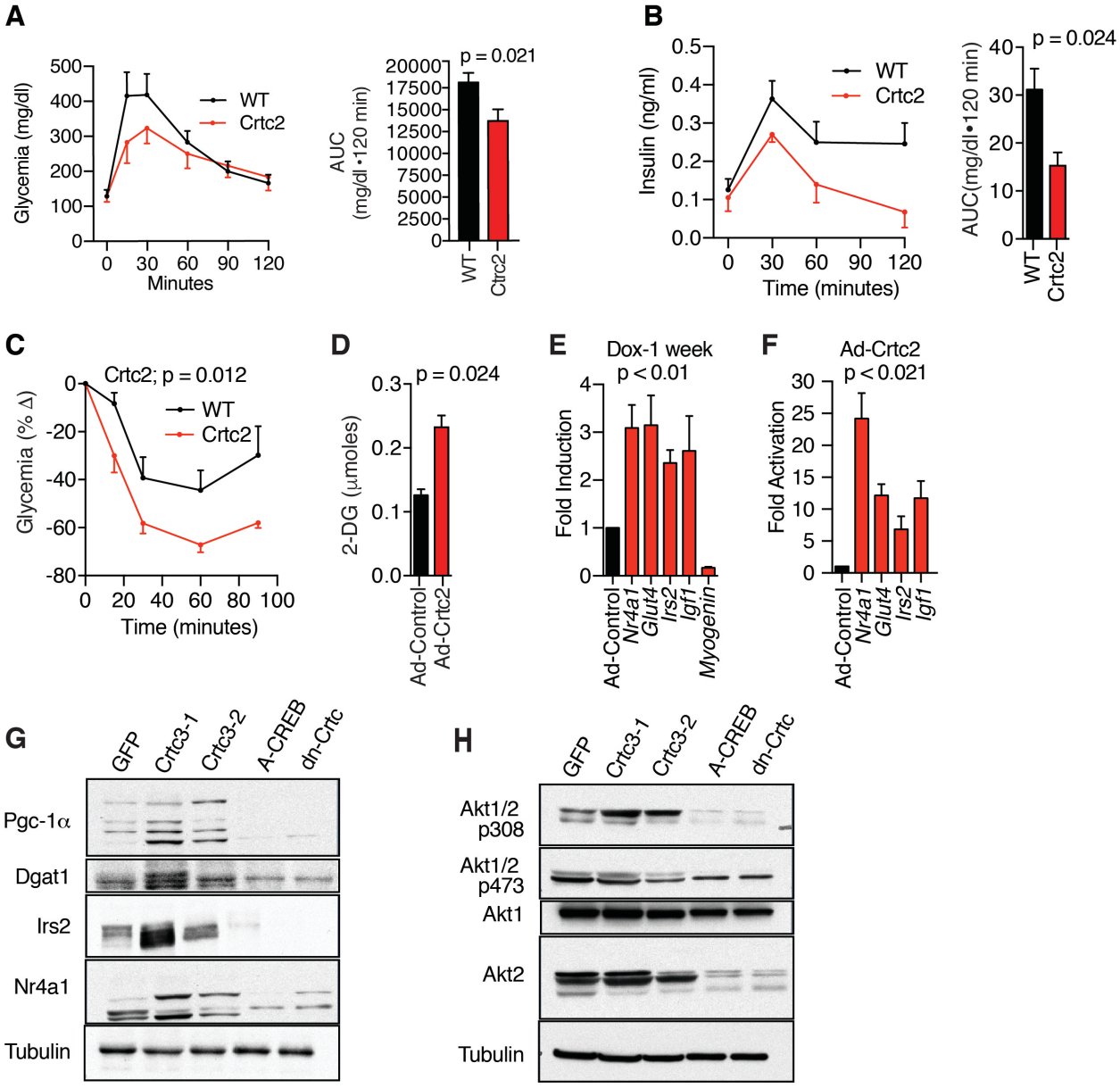

Figure 2. Crtc2 transgenic mice maintain enhanced glucose disposal and insulin tolerance

(**A**) Glucose tolerance test (GTT). Right panel, area under the curve. *N* = 10 mice per group

(**B**) Plasma insulin levels during GTT described in panel **B**.

(**C**) Insulin tolerance tests. *N* = 10 mice per group

(**D**) Insulin-mediated uptake of 2-deoxy-D-glucose in primary myocytes transduced with adenovirus expressing Crtc2 or GFP control. *N* = 10 per group. Student's t-test.

(**E**) Crtc2 mice were treated +/- dox for 1 week and the gene induction compared by qPCR relative to the no dox groups. N= 10 per group.

(**F**) Gene expression in primary myocytes transduced with adenovirus expressing Crtc2 or GFP

628 control were compared by qPCR. *N*=4 per group.

629 **(G–H**) Myocytes stably expressing GFP, Crtc3 (lanes 2 and 3), dominant negative Creb (A-

630 CREB), or dominant negative Crtc2 (dn-Crtc) were compared by western blots.

631 Data are mean ± SEM.

632

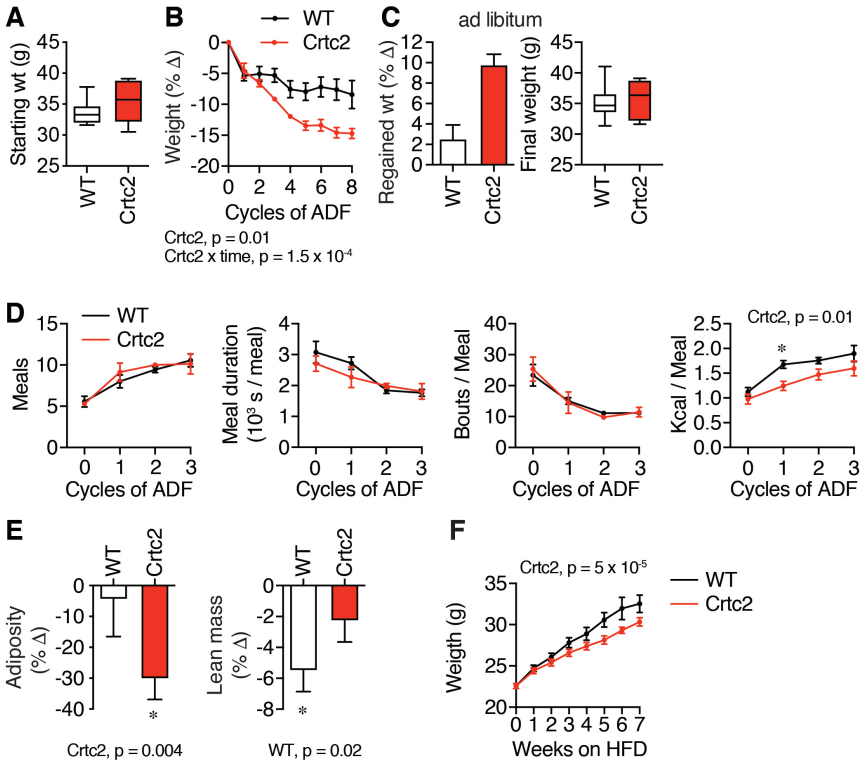

Figure 3. Crtc2/Creb1 signaling enables greater loss of weight and adiposity during alternate day fasting (ADF).

(**A**) 18-week old C57BL/6 male control (WT) and Crtc2 mice were treated with dox for 35 days and weighed. Data are shown as box-and-whisker plot, indicating the middle quartiles and range. $N = 6$ (WT) or 5 (Crtc2) mice per group.

(**B-E**) Mice from (**A**) were subject to alternate day fasting (ADF).

(**B**) Changes in the body weight during ADF.

(**C**) Weight regain after the ADF treatment and 3 weeks of ad libitum feeding.

(**D**) Behaviors were assayed with Biodak monitoring system, including number of meals, bouts per meal, meal duration, and kilocalories consumed over the 12-hr re-feeding period. *significant in Sidak's test for planned comparisons.

(**E**) Adiposity and lean mass determined by whole-body NMR measurements taken before and after 8 cycles of ADF. Data analyzed with 1-way ANOVA

(**F**) 8-week old C57BL/6 male control and Crtc2 mice were treated with dox and placed on a high fat diet (HFD). $N = 9$ (WT) or 7 (Crtc2) mice per group

Time course data was analyzed by 2-way ANOVA. Data are shown as mean ± SEM.

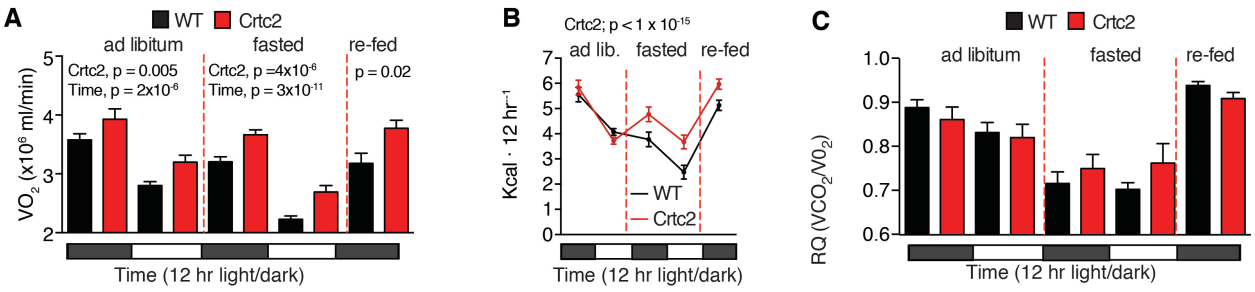

Figure 4. Whole-body energy expenditure is reduced by weight loss and fasting and is reversed by Crtc2 expression.

(**A**) VO_2 and VCO_2 were measured continuously (**Figure S2A**) for 72 hrs. in a CLAMS animal monitoring system. Shown are the 12-hr averages. $N = 8$ mice per group.

(**B**) Total energy expenditure was calculated from VO_2 and VCO_2 values using the Lusk equation.

(**C**) The respiratory quotient (RQ) was determined during the CLAMS experiment.
Data are shown as mean ± SEM and were analyzed by 2-way ANOVA for the different feeding conditions separately.

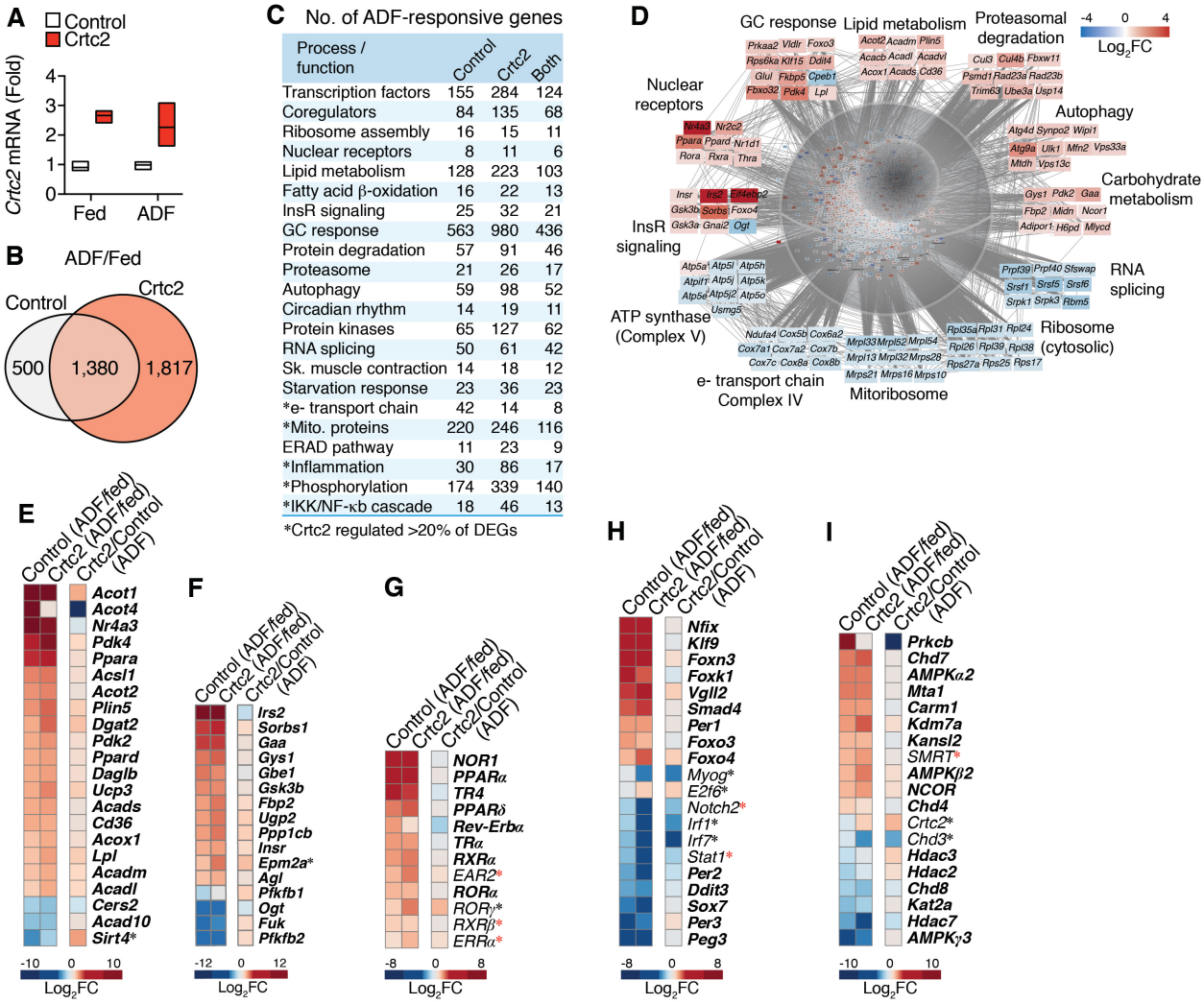

Figure 5. Transcriptional control of fasting and weight loss and its regulation by Crtc2.

(**A**) Mice TA muscles were transduced with GFP control or Crtc2 expression vector. Crtc2 mRNA levels in the TA of mice fed ad libitum (Fed), or subject to ADF (Fast) were compared by qPCR. $N = 3$ mice per group.

(**B**) Venn diagram showing the numbers of DEGs identified by mRNA-seq comparing the effects of ADF in control versus Crtc2-transduced TA muscles.

(**C**) Biological processes and functions regulated by ADF and Crtc2. Gene ontology (GO) analysis suggests that ADF regulates several processes/ functions in a Crtc2-sensitive manner. The numbers of DEGs involved in each process are shown. See SI Appendix, **Dataset S1** for a

675 complete list of represented GO annotations.

676 (**D**) Examples of ADF-regulated transcriptional programs and mRNAs in control TA muscles.

677 (**E–I**) Gene expression profiles in control and Crtc2-transduced TA muscles of mice subjected to

678 ADF relative to the ad libitum fed mice (columns 1–2), and effect of Crtc2 transduction relative

679 to control during ADF (column 3). Expression profiles of genes that encode **E**) nuclear

680 receptors, **F**) other transcription factors, **G**) transcriptional coregulators, **H**) regulators of lipid

681 metabolism, and **H**) regulators of carbohydrate metabolism. . ADF-regulated genes in control

682 muscle appear in **bold**. *Crtc2-regulated genes in mice subjected to ADF. *ADF-regulated

683 genes in Crtc2-transduced muscle but not control. FC, fold change.

684

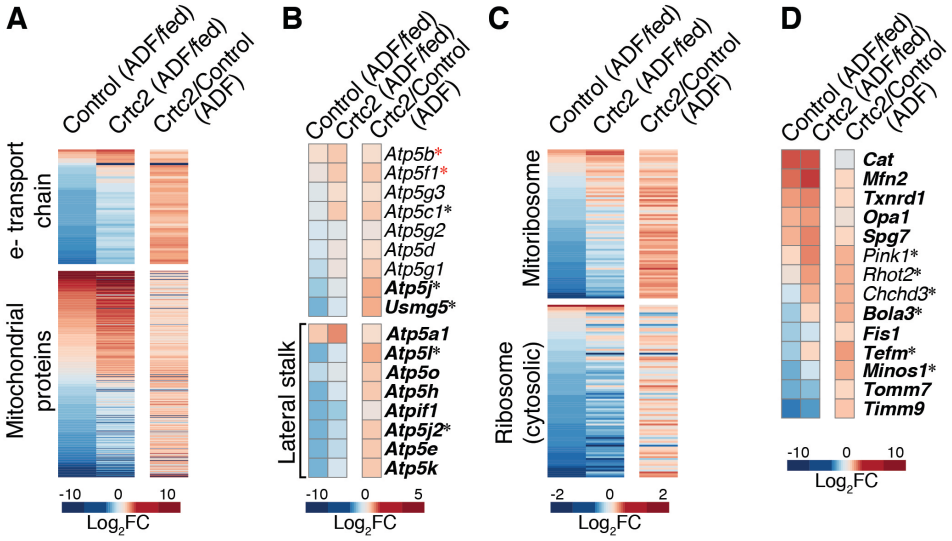

Figure 6. Alternate day fasting and Crtc2 regulation of mitochondrial gene expression. **A–D)** Gene expression profiles in control and Crtc2-transduced TA muscles of mice subjected to ADF relative to the ad libitum fed mice (columns 1–2), and effect of Crtc2 transduction relative to control during ADF (column 3). The profiles of all genes encoding **A**) mitochondrial proteins, including subunits of electron transport chain (ETC) complexes, **B**) subunits of the mitochondrial ATPase (complex V), **C)** ribosomal subunits, and **D**) highlighted mitochondrial proteins, are shown. ADF-regulated genes in control muscle appear in **bold**. *Crtc2-regulated genes in mice subjected to ADF. *ADF-regulated genes in Crtc2-transduced muscle but not control. FC, fold change.

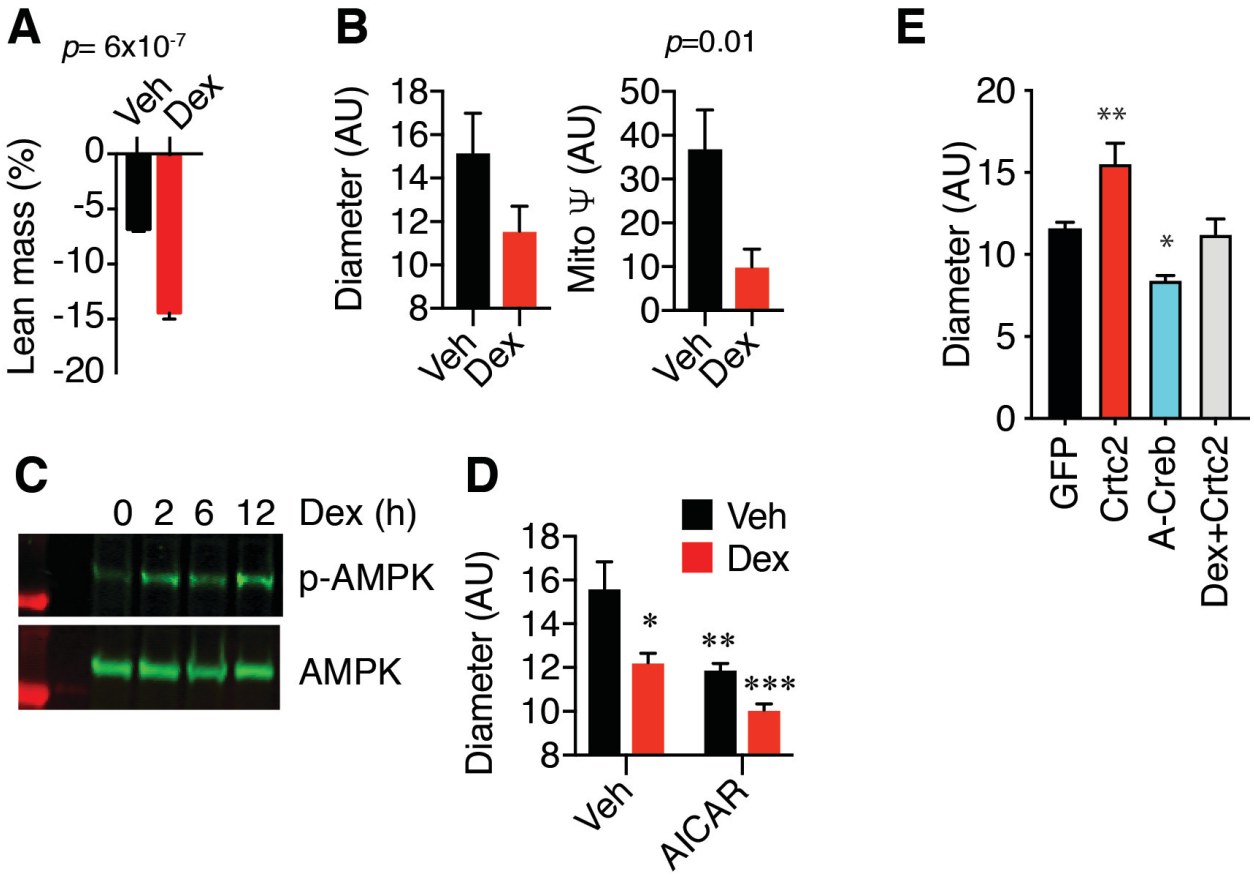

Figure 7. Glucocorticoids and AMPK regulate skeletal muscle atrophy and mitophagy.

(**A**) Effects of Dex on lean body mass. Mice injected with vehicle or 10 mg/kg Dex were fasted overnight. Lean mass was measured by whole-body NMR before and after treatment. *N* = 5 mice per group.

(**B**) Diameter and mitochondrial potential of steroid-deprived primary myotubes treated for 2 days with vehicle or 100 nM Dex were compared by confocal high-content imaging. *N* = 24–27 images x 50–100 myotubes per image.

(**C**) Steroid-deprived C_2C_{12} myotubes were stimulated with 100 nM Dex for 0–12 h. Levels of phosphorylated and total AMPK in whole lysates were compared by western blot.

(**D**) Diameter of steroid deprived C_2C_{12} myotubes treated for 48 h with vehicle, 100 nM Dex, or 1 uM AICAR were compared by confocal high content imaging. *N* = 24–27 images x 50–100 myotubes per image.

(**E**) C2C12 myocytes were transduced with adenovirus GFP, Crtc2, or A-Creb genes and analyzed by confocal high content imaging. *N* = 24–27 images x 50–100 myotubes per image.

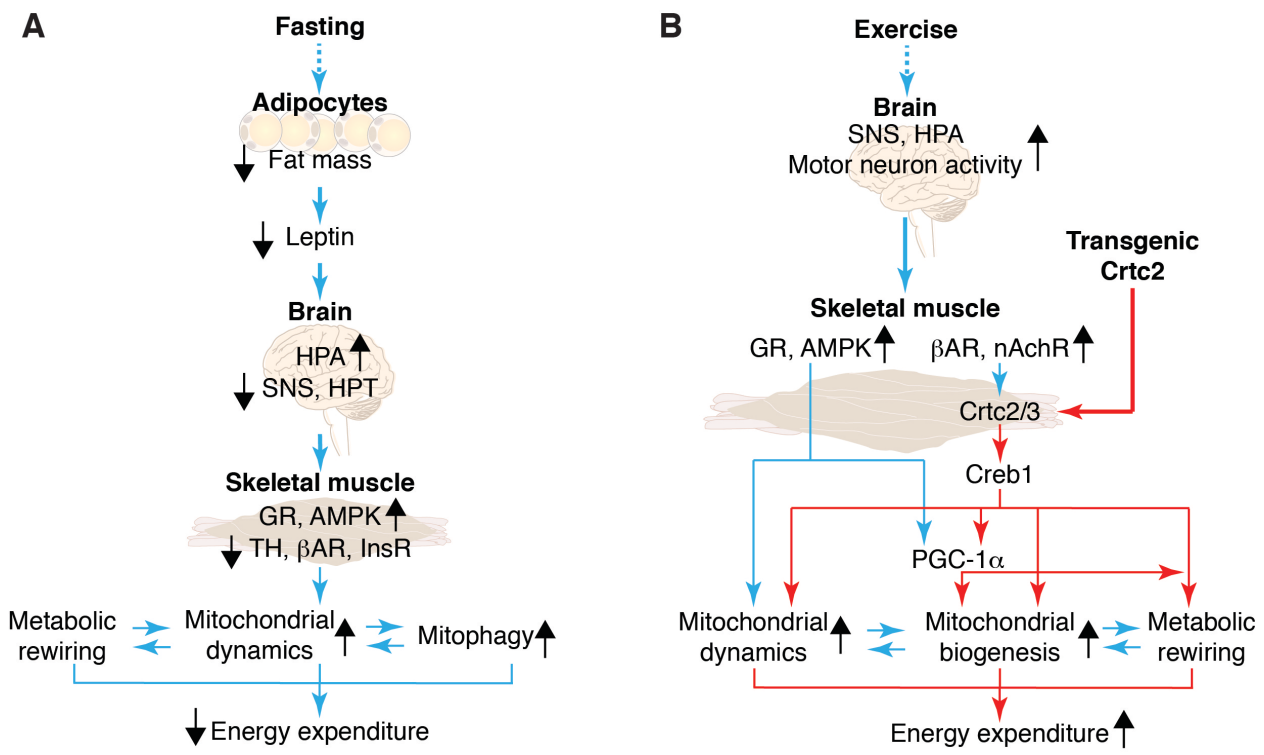

Figure 8. Hormonal and neural modulation of energy expenditure in skeletal muscle

(**A**) Fasting-induced regulation of mitochondrial dynamics and mitophagy.

(**B**) Exercise-induced regulation of mitochondrial dynamics and mitochondrial biogenesis, which can be constitutively activated by overexpression of Crtc2 in skeletal muscle.

bAR, b-adrenergic receptor; GR, glucocorticoid receptor; HPA, hypothalamic-pituitary-adrenal axis; HPT, hypothalamic-pituitary-thyroid axis; InsR, insulin receptor; nAchR, nicotinic acetylcholine receptor; SNS, sympathetic nervous system; TH, thyroid hormone

724 Supplemental Information for

725

726 **Activation of the Crtc2/Creb1 transcriptional network in skeletal muscle enhances weight**

727 **loss during intermittent fasting**

728 Nelson E. Bruno[1]*, Jerome C. Nwachukwu[1], Sathish Srinivasan[1], Richard Hawkins, David

729 Sturgill[3], Gordon L. Hager[3], Stephen Hurst[4], Shey-Shing Sheu[4], Michael D. Conkright[5], Kendall

730 W. Nettles[1]*

731

732 Correspondence: Nelson E Bruno, nbruno@scripps.edu; Kendall Nettles, knettles@scripps.edu

733

Pathway name	# Entities found	# Entities total	FDR
Extracellular matrix organization	45	329	3.98E-14
Assembly of collagen fibrils and other multimeric structures	17	67	2.12E-14
MET promotes cell motility	10	45	5.98E-07
Elastic fibre formation	12	46	6.13E-11
Regulation of Insulin-like Growth Factor (IGF) transport and uptake	13	127	2.47E-05
Neutrophil degranulation	26	480	2.35E-05
Immune System	79	2823	7.75E-06
Signaling by Receptor Tyrosine Kinases	23	622	7.13E-04
Signaling by Interleukins	25	639	0.049

Supplemental Table 1. Gene pathway enrichment for secreted proteins among DEGs regulated by Crtc2 during ADF.

734

735

736 **Supplemental Figures**

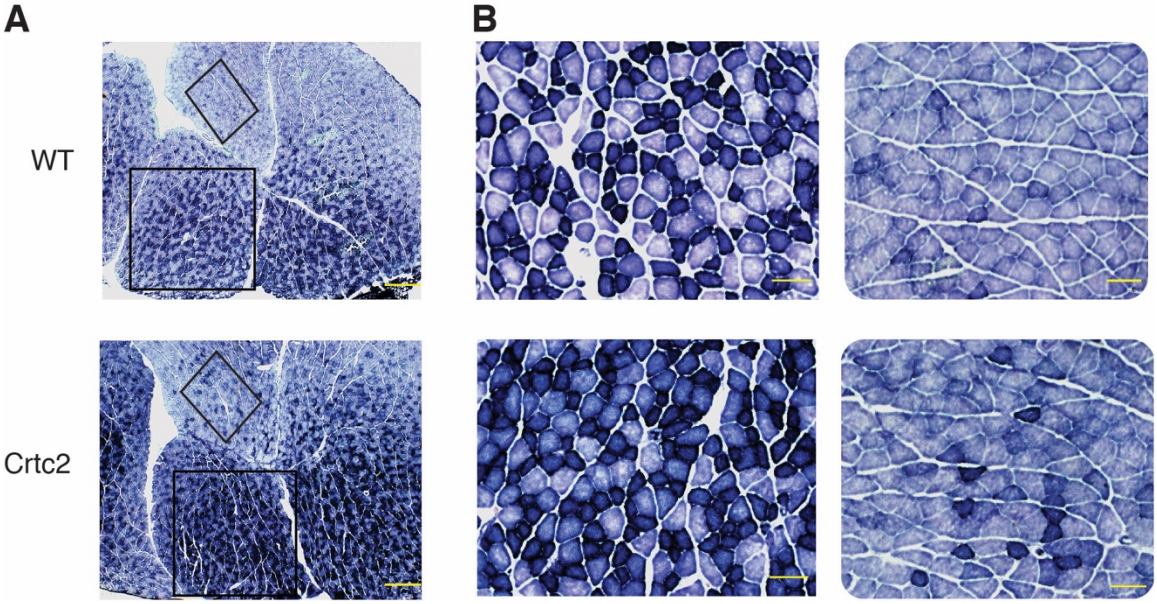

737

738 **Supplemental Fig 1. Analysis of succinate dehydrogenase in skeletal muscle fibers.**
739 (**A–CB**) Histological analysis of succinate dehydrogenase in myofibers from gastrocnemius
740 muscle sections of WT and Crtc2 mice after Dox treatment. Boxes highlight areas of lighter
741 and darker staining **B**) Scale bar = 2 mm. **C**) Scale bar = 100 µm. Close up from boxed areas
742 in **B**)
743

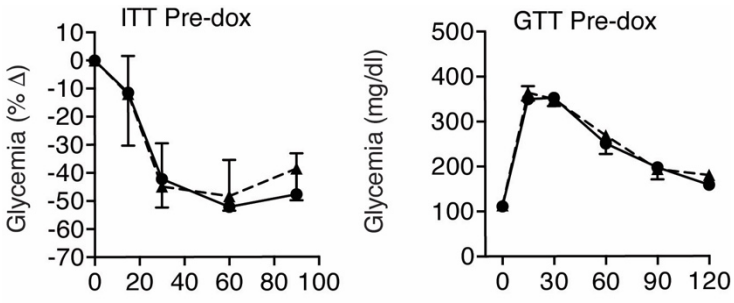

Supplemental Fig. 2. Glucose tolerance test controls

(**C–D**) GTT on WT and Crtc2 transgenic animals treated with dox for 1 week. Mice were fasted for 16 hrs. before i.p. injection of 20% glucose. n =10 mice per group.

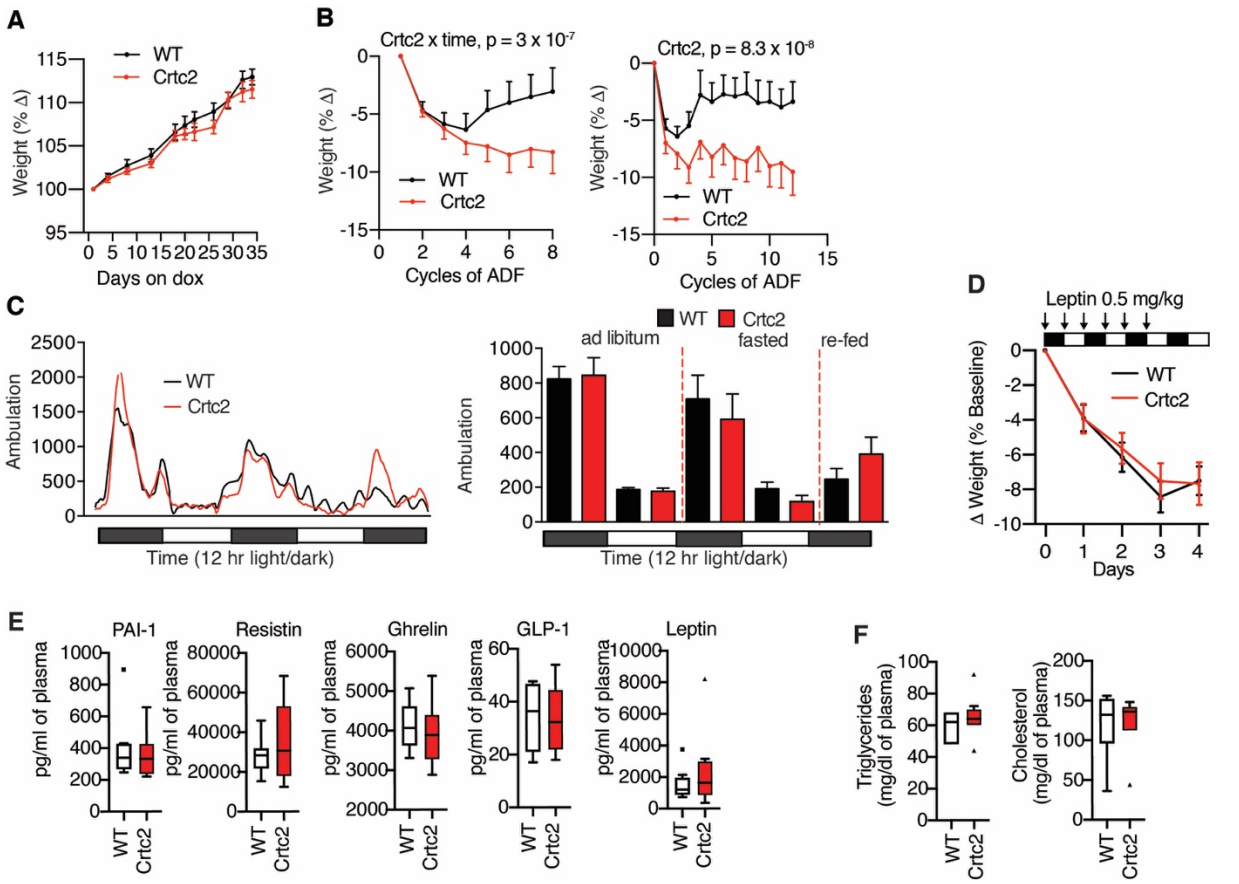

Supplemental Fig. 3. Effects of skeletal muscle overexpression of Crtc2 on the response to ADF and plasma feeding hormones in Crtc2 mice fed ad libitum.

(**A**) Weight gain after treatment of 18-week old WT and Crtc2 transgenic mice (n=8) with doxycycline.

(**B**) Changes in body weight during ADF.

(**C**) Average ambulatory activity during ad libitum feeding, fasting and re-feeding, n = 8 mice per group. 12-hr averages of the data. There were no significant effects of Crtc2. **A–C)** Data shown as mean ± SEM.

(**D**) WT or Crtc2 mice were injected twice daily with 0.5 mg/kg leptin and weight was monitored. *N*=8 mice per group.

(**E–F**) Analysis of plasma proteins regulating feeding and triglycerides and cholesterol in Crtc2 expressing and WT mice.

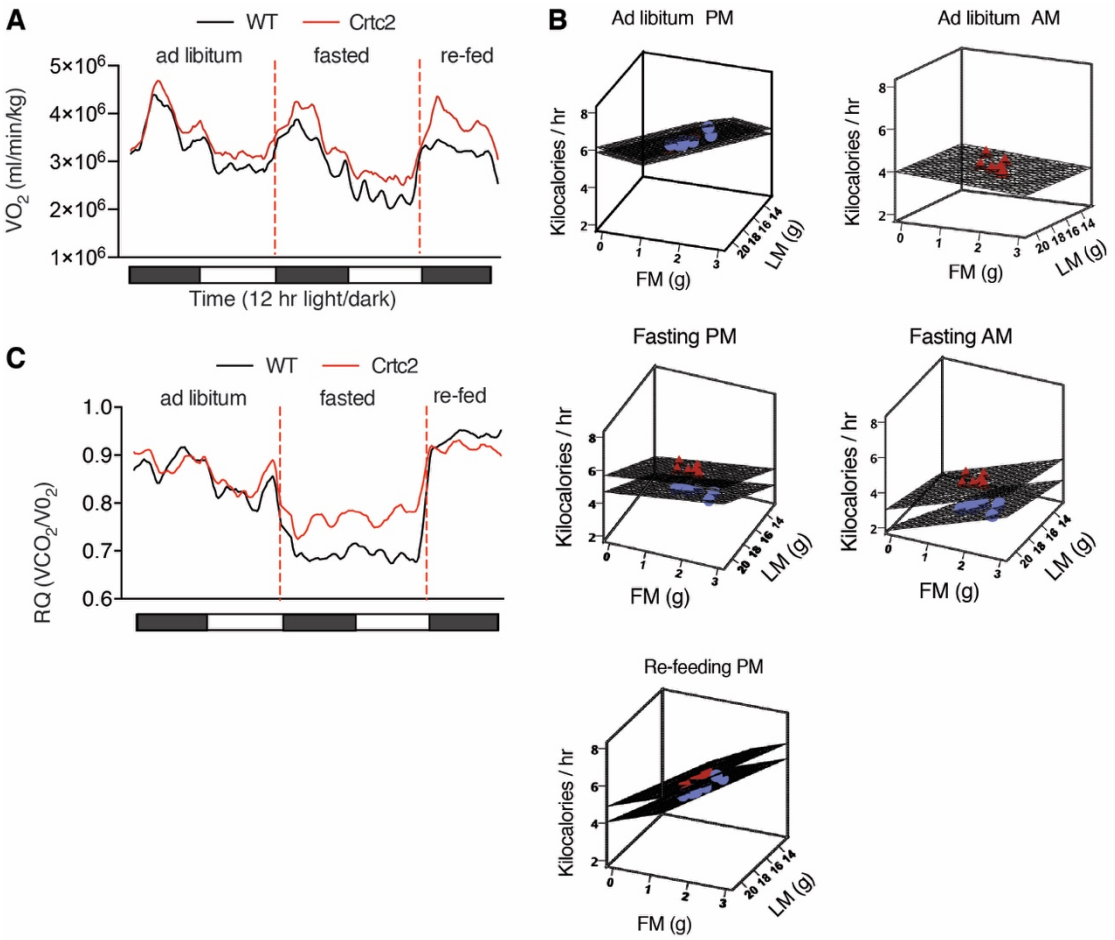

765

766 **Supplemental Fig. 4 Whole-body energetics.**

767 (**A**) VO_2 (and VCO_2) were measured continuously for 72 hrs. in a CLAMS animal monitoring
768 system during alternate day fasting. N = 8 per group

769 (**B**) Total energy expenditure (EE) for WT and Crtc2 mice was calculated from VO_2 and VCO_2.
770 The data was adjusted by repeated measures ANCOVA in with lean mass (LM) and fat mass
771 (FM) as covariants at the following values: LM = 17.01 g; and FM = 1.62 g. Dot plot graphs
772 shows adjusted means derived from repeated measure general linear model ANCOVA, using
773 5 consecutive 12-hr time intervals: PM-ad libitum; AM-ad libitum; PM-Fast; AM-Fast; and
774 Re-feed EE as dependent variables, and LM and FM as covariates. The lack of intersection of
775 the planes graphically demonstrates lack of covariation.

776 (**C**) Respiratory Quotient from CLAMS experiment during alternate day fasting.

777 Data are mean +SEM.

778

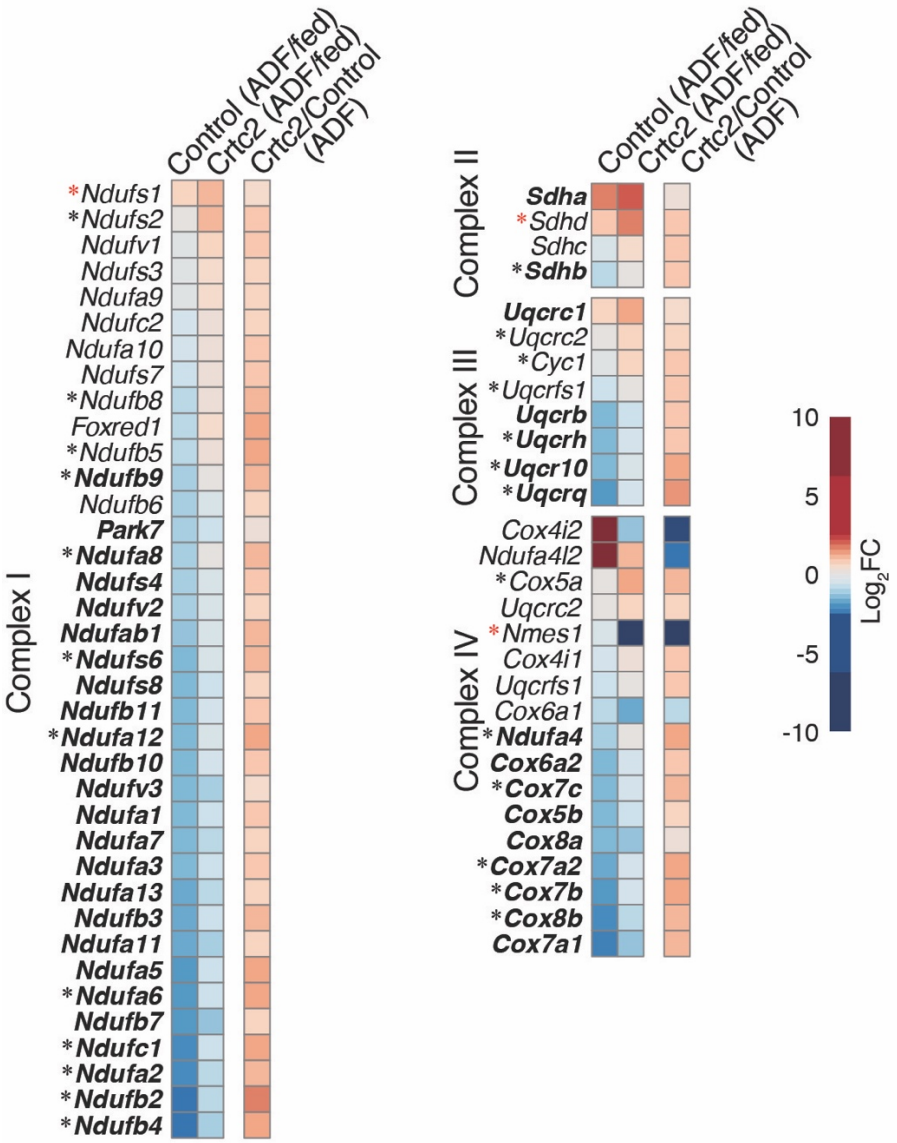

Supplemental Fig. 5 Electron transport chain gene expression

Expression profiles of genes that encode the electron transport chain. The mRNA levels in control and Crtc2-transduced TA muscles of mice subjected to ADF relative to the ad libitum fed mice (columns 1–2), and effect of Crtc2 transduction relative to control during ADF (column 3) are shown. ADF-regulated genes in control muscle appear in **bold**. *Crtc2-regulated genes in mice subjected to ADF. *ADF-regulated genes in Crtc2-transduced muscle but not control. FC, fold change